



## Full Length Article

## Zingiber officinale-Mediated biosynthesis of bimetallic Gold/Silver (BAu/Ag) nanoalloys; an insight into antiviral and anticancer activities

Khalid S. Alshallash<sup>a</sup>, Ahmed M. Eid<sup>b</sup>, Saad El-Din Hassan<sup>b</sup>, Mohammed Ali Abdel-Rahman<sup>b</sup>, Abdullah S. Alawam<sup>a</sup>, Mohammed F. Hamza<sup>c,d</sup>, Amr Fouda<sup>b,\*</sup>

<sup>a</sup> Department of Biology, College of Science, Imam Mohammad Ibn Saud Islamic University (IMSIU), Riyadh 11623, Saudi Arabia

<sup>b</sup> Botany and Microbiology Department, Faculty of Science, Al-Azhar University, Nasr City, Cairo 11884, Egypt

<sup>c</sup> School of Nuclear Science and Technology, University of South China, Hengyang 421001, China

<sup>d</sup> Nuclear Materials Authority, P.O. Box 530, El-Maadi, Cairo 11728, Egypt



## ARTICLE INFO

## Keywords:

Green synthesis  
Nanoalloys  
Bimetallic  
Antiviral  
In-vitro cytotoxicity

## ABSTRACT

Utilizing plant extracts in the green synthesis of bimetallic nanoalloys receives more attention due to its eco-friendly, cheap, single-step, easy-handling method, producing highly active and biocompatible nanoalloys. Therefore, the aqueous extract of ginger rhizome was used to form bimetallic gold/silver (Au/Ag) nanoalloys. There were 37.3 mg.g<sup>-1</sup> of total soluble carbs, 0.75 mg.g<sup>-1</sup> of proteins, and 0.03 mg.g<sup>-1</sup> of phenolic compounds quantified in ginger rhizome. The production of BAu/Ag-NPs relies on these components. The as-formed BAu/Ag-NPs were characterized using UV-Vis spectroscopy. The results showed that the peak surface plasmon resonance (SPR) occurred between 440 and 545 nm. The existence of several functional groups involved in the reduction and stability of the generated nanoalloys was shown by Fourier-transform infrared (FT-IR). The nanoalloys, with an average size of 49.1 ± 16.2 nm, were observed to be spherical using transmission electron microscopy (TEM). Energy-dispersive X-ray (EDX) indicated that the synthesized nanoalloy mainly consisted of Au and Ag ions, which made up (31.2 % and 47.1 %) and (45.9 % and 28.6 %) of the sample's atomic and weight percentages, respectively. The crystallography of the nanoalloys was confirmed using XRD analysis. When examined for their capacity to suppress viral replication, the synthesized nanoalloys showed remarkable results, with 78.2 % inhibition against HAV and 69.6 % against Cox-B4. In addition, the anticancer activity of nanoalloys against oral epithelial cells (OEC), MCF7 adenocarcinoma cells, and HepG2 hepatocarcinoma cells was investigated using the MTT assay method. While the nanoalloys exhibited moderate toxicity towards normal OEC (IC50: 502.5 ± 2.8 g.mL<sup>-1</sup>), they showed substantial cytotoxicity towards cancer cells, MCF7 and HepG2, with IC50 values of 212.6 ± 4.4 and 117.9 ± 6.6 µg.mL<sup>-1</sup>, respectively. According to these data, BAu/Ag nanoalloys show potential as antiviral and anticancer drugs that selectively kill cancer cells.

## 1. Introduction

Rapid developments in nanotechnology have broad ramifications for fields as diverse as electronics and medicine (Malik et al., 2023). Among the myriad of nanoparticles that have emerged, bimetallic gold (Au)/silver (Ag) nanoalloys are all the rage now because of their unique and synergistic properties originating from the combination of Au and Ag (Makada et al., 2023). Because of their unique properties, they integrated into various fields like biomedicine and beyond. Traditional chemical and physical methods for producing nanomaterials necessitate using toxic chemicals, significant amounts of energy, and labor-

intensive procedures. Conventional nanoparticle production methods pose risks to the surrounding environment and the people working on the project (Nassar et al., 2023). Exploring green and sustainable synthesis pathways has emerged as a significant research direction to solve these issues (Khademi-Azandehi and Moghaddam, 2015). Eco-friendly manufacturing of bimetallic Au/Ag nanoalloys is possible using plant and microbial extracts to act as dual functions, bio-reducing, and capping agents (Hamza et al., 2022, Singh et al., 2022).

Ginger (*Zingiber officinale*), a well-known medicinal plant with a rich phytochemical composition, has brought widespread notice as a spice and herbal treatment. Flavonoids, phenolic compounds, and terpenoids

\* Corresponding author.

E-mail address: [amr\\_fh83@azhar.edu.eg](mailto:amr_fh83@azhar.edu.eg) (A. Fouda).

<https://doi.org/10.1016/j.jksus.2024.103243>

Received 24 December 2023; Received in revised form 6 May 2024; Accepted 7 May 2024

Available online 8 May 2024

1018-3647/© 2024 The Authors. Published by Elsevier B.V. on behalf of King Saud University. This is an open access article under the CC BY-NC-ND license (<http://creativecommons.org/licenses/by-nc-nd/4.0/>).

are only some of their bioactive components (Mao et al., 2019). Ginger extract is a promising material for NP synthesis because it contains chemicals with strong reducing properties, such as gingerol and zingerone (Hu et al., 2022). This research uses ginger extract's reducing ability to speed up bimetallic Au/Ag nanoparticle synthesis. Benefits such as reduced environmental impact and the absence of dangerous chemicals are just the tip of the iceberg for this biogenic synthesis method, which serves as a paradigm for green chemistry. The formation of nanoparticles by metal ion reduction starts with the interaction of metal ions with different active molecules in the ginger extract (Eid et al., 2023).

Bimetallic nanoalloys, consisting of two or more metals, can exhibit a wide variety of characteristics not seen in monometallic nanoparticles. In the case of Au and Ag, combining their distinct properties produces a synergistic amalgam with augmented functions. The remarkable catalytic performance of Au/Ag nanoalloys stands out most prominently. When combined, Au and Ag have synergistic effects that boost catalytic activity in processes like organic molecules' oxidation–reduction and contaminants' oxidation. Environmental restoration and sewage treatment are just two examples of the many important uses for these catalytic characteristics (Wang et al., 2019). Also, photothermal treatment (PTT) has shown promising results using bimetallic Au/Ag nanoalloys. PTT is a method for treating cancer in which near-infrared (NIR) light is used to cause nanoparticles to generate heat. This process produces localized hyperthermia and can be used to ablate cancer cells successfully. Au/Ag nanoalloys are promising candidates for PTT applications due to their exceptional optical characteristics (Han and Choi, 2021). In addition to their applications in diagnostics and therapy, bimetallic Au/Ag nanoalloys have demonstrated synergistic antibacterial properties. They are highly efficient against many types of bacteria, including those that have developed resistance to antibiotics. Advanced wound dressings, coatings for medical devices, and tailored antibacterial medicines all require this quality (Rabiee et al., 2022). We expect the creation of cutting-edge biomedical applications that fully utilize the benefits of bimetallic Au/Ag nanoalloys to advance human health as research in this area continues to grow.

The novelty of the above data lies in the biosynthesis and characterization of Ag/Au nanoalloys using a novel surface modification technique or composition. Despite the previous reports on the anticancer/antibacterial activity of Ag/Au nanoalloys, this study introduces a cost-effective, eco-friendly, and biocompatible approach to enhance the biological activities of the nanoalloys. This could include innovative synthesis methods using plant extracts integrated into novel biomedical applications. By elucidating the specific advancements or modifications made in the synthesis and characterization processes, the current investigation demonstrates how this work extends beyond existing literature and contributes to the field's advancement, thereby highlighting the novelty of the reported findings.

Therefore, this investigation uses ginger extract as an eco-friendly and sustainable technique for manufacturing bimetallic Au/Ag nanoalloys. UV–Vis spectroscopy, Transmission electron microscopy (TEM), Fourier-transform infrared (FT-IR), X-ray diffraction (XRD), and Energy-dispersive X-ray spectroscopy (EDX) were used to rigorously characterize the morphological and structural/compositional characteristics of the synthesized nanoparticles. It also explores the possible medical applications of nanoalloys, including antiviral and anticancer activity, and their many unique characteristics.

## 2. Materials and methods

### 2.1. Materials

Chloroauric acid (HAuCl<sub>4</sub>, 99 %) and silver nitrate (AgNO<sub>3</sub>, 98 %) were purchased from Sigma Aldrich in Darmstadt, Germany to be utilized as metal precursors. All components used in the culture media were obtained from Sigma Aldrich in Cairo, Egypt. The cancer, normal cell

lines, and viral strains utilized in this study were obtained from the Holding Company for Biological Products and Vaccines (VACSERA), Cairo, Egypt. All the reactions were conducted using distilled water (dH<sub>2</sub>O).

### 2.2. Detection of secondary metabolites in the ginger rhizome (*Zingiber officinale*)

The contents of ginger rhizome aqueous extract from total carbohydrates, proteins, and phenols were analyzed. These metabolites play an important role in the formation of bimetallic nanoparticles. The total soluble carbohydrate content in the ginger rhizome was measured based on the method of Umbreit et al. (Umbreit and Stauffer, 1957). In contrast, the soluble protein contents were detected according to the lowery method. On the other hand, the total phenols were estimated using the spectroscopic method, according to Annisworth and Gillespie (Ainsworth and Gillespie, 2007).

### 2.3. Biosynthesis of bimetallic Au/Ag nanoalloy (BAu/Ag-NPs) using *Zingiber officinale*

Ginger rhizome (*Zingiber officinale*) was obtained from a local Egyptian supermarket. Three separate washes in running water were used to remove any adhering traces of dirt or dust from the surface. Then, we added 100 mL of dH<sub>2</sub>O to 10 g of rhizome cut into smaller pieces. For 60 min, this mixture was kept at 100 rpm, and 60 °C. Following a 10-minute centrifuge at 1,000 rpm, the resultant supernatant was collected for a green synthesis of Au/Ag nanoalloys.

Biosynthesized BAu/Ag-NPs were achieved with a ratio of 1: 1 as follows: 40 mL of HAuCl<sub>4</sub> stock solution (1 mM) was introduced into 20 mL of collected plant aqueous extract, followed by stirring the mixture at 60 °C for 60 min. The final concentration for the bimetallic Au/Ag nanoalloy (1 mM) was achieved by adding 40 mL of a one mM AgNO<sub>3</sub> stock solution dropwise to the prior mixture. The pH of the solution (8.0) was adjusted using 1 M NaOH solution. Changing the plant aqueous extract from pale yellow to reddish-purple indicates the formation of BAu/Ag-NPs after 60 min. The obtained solution was kept overnight at room temperature to confirm complete metal reduction as indicated by a stable color. After that, the formed BAu/Ag-NPs colloidal solution was oven-dried (200 °C for 6 h). For more purification, the residue was washed twice with dH<sub>2</sub>O before collection (Salem et al., 2020).

### 2.4. Characterization

The color shift is the first indicator that the green synthesis of BAu/Ag-NPs utilizing the ginger extract was effective. Hence, the solution absorbance was measured at 200–800 nm to determine the strength of the reddish-purple using JENWAY 6305 Spectrophotometer (Staffordshire, UK). The analysis was performed by adding two milliliters of the newly synthesized solution to a quartz cuvette and recording spectral readings at regular time intervals to determine the maximum SPR point. The functional groups present in the ginger extract having a role in the formation of BAu/Ag-NPs were explored using Agilent FT-IR (Cary 630 model) spectroscopy at the range of wavenumbers of 400–4000 cm<sup>-1</sup>. Moreover, TEM and EDX analyses were conducted to investigate the shape, size, and complementary mapping of BAu/Ag-NPs. These analyses were conducted using a JEOL 1010 TEM and JEOL JSM-6360LA EDX (JEOL, Japan). Before sample preparation, the noncolloidal aqueous suspension underwent sonication for several minutes. Sample preparation involved depositing a drop of the primary sample onto a copper grid coated with a perforated carbon film, which subsequently underwent drying at 80 °C to a 6 h in an oven (Amin et al., 2021). The synthesized BAu/Ag-NPs crystallinity was explored through XRD using an X'Pert PRO instrument (Philips, Eindhoven, Netherlands) at a 2θ range of 10°–80°. Scanning was conducted at 40 kV (voltage) and 30 mA (current) using a Cu Kα X-ray source. The average size was determined

using Scherrer's equation.

$$D = \frac{K\lambda}{\beta \cos\theta} \quad (1)$$

whereas D, is the average crystallite size; K, is the Scherrer constant (0.94);  $\lambda$ , is the source of X-ray wavelength that is equal to 1.54;  $\beta$ , is half of the maximum intensity; and  $\theta$ , is Bragg's diffraction angle.

## 2.5. Antiviral activity

### 2.5.1. Detect the cytotoxic efficacy of BAu/Ag-NPs on Vero cells by MTT assay method

The Vero cells (normal cells as host cells) were used to determine the maximum non-toxic concentration (MNTC) of the green synthesized BAu/Ag-NPs through implementation into a 96-well plate. In this method, the Vero cells at a concentration of  $10^4$  cells/well in 100  $\mu$ L of growth media were incubated at 37°C for 24 h in a CO<sub>2</sub> incubator (5 %) till forming a confluent Vero cells sheet. After that, the growth media was removed, and the attached Vero cells with double-fold BAu/Ag-NPs concentrations were 1000 to 31.25  $\mu$ g·mL<sup>-1</sup>. DMSO was used as a solvent, and the test was conducted in triplicate for each concentration. The positive control was represented as cells without any treatment. The plates containing cells and nanoparticles were incubated at 37°C for 48 h in a CO<sub>2</sub> incubator (5 %). At the end of the incubation period, the plates were checked for any harmful signs such as monolayer disruption, cell granulation, rounding, and shrinking by an inverted microscope. To each well, 20  $\mu$ L of MTT solution (5 mg mL<sup>-1</sup> in phosphate buffer) was added, mixed by shaking at 150 rpm for 5 min, and then incubated at 37 °C for 5 h in a CO<sub>2</sub> incubator. After that, the well content was discarded, and 200  $\mu$ L DMSO was added to dissolve the formed formazan crystals (MTT metabolic product) in each well. The optical density (OD) was measured at 570 nm by ELIZA microplate readers.

Cell viability was calculated as follows:

$$\text{Cell viability (\%)} = \frac{A_t}{A_c} \times 100 \quad (2)$$

whereas  $A_t$  is the treatment absorbance; and  $A_c$ , is the control absorbance. Whereas the cell toxicity was calculated as the following:

$$\text{Cell toxicity (\%)} = \text{cell viability} - 100 \quad (3)$$

The toxicity (%) and the concentrations of BAu/Ag-NPs were graphed, with toxicity percentages on the Y-axis and BAu/Ag-NPs concentrations on the X-axis. This graph allowed the determination of the MNTC (the nanoparticle concentration that maintains the cell viability of host cells, such as Vero cells, without significant difference compared to control) for assessing antiviral activity. Additionally, the CC50 (the concentration of the nanoalloy inhibiting 50 % of the growth of Vero cells compared to untreated cells) was calculated using regression analysis.

### 2.5.2. Antiviral assay

The antiviral effect of BAu/Ag-NPs alloy was investigated using hepatitis A virus (HAV) and Coxsackie B virus (Cox-B4). At first, the Vero cells (host cells) were cultivated as mentioned above till forming a confluent sheet. At the same time, the viral suspension was incubated with non-toxic nanoparticle concentration (1:1, v/v) for one hour at 35  $\pm$  2 °C. After that, 100  $\mu$ L of the last mixture (viruses and BAu/Ag-NPs) was added to each well. The control (non-infected cells) was represented as the three wells containing only Vero cells. The plates were mixed well by shaking at 150 rpm for five minutes before being incubated overnight at 37°C in 5 % CO<sub>2</sub>. The assessment of viability in both control and infected Vero cells involved the quantification of formazan crystal absorbance following the addition of MTT solution, as described earlier. Antiviral activity was determined by evaluating the disparity between the optical density values of the viability of the control group and

infected cells (Abdel-Rahman et al., 2024).

## 2.6. Anticancer assay

In-vitro cytotoxicity testing of BAu/Ag-NPs alloy biosynthesized using ginger aqueous extract was performed on OEC (normal oral epithelial cell), MCF7 (adenocarcinoma), and HepG2 (hepatocellular carcinoma) cell lines using the MTT assay. After incubation CO<sub>2</sub> incubator (5 %) for 24 h at 37 °C, the cells were harvested from the tissue culture plates. After forming monolayers, the cells were rinsed twice with a washing solution, then exposed to BAu/Ag-NPs at concentrations 31.25–1000  $\mu$ g mL<sup>-1</sup> for 48 h; three wells served as controls (without nanoparticles treatment). The incubation media was removed, and 5 mg mL<sup>-1</sup> of MTT solution (dissolved in phosphate-buffered saline PBS) was added to each well and mixed for 5 min. The plates were then incubated for another four hours at 37 °C with aluminum foil covering them. The MTT solutions were drained after incubation to dissolve the formazan crystals, and then 100  $\mu$ L of DMSO (10 %) was added. After 30 min of shaking in the dark, the plate's absorbance was measured at 570 nm using an ELISA reader (Ghasemi et al., 2021). The cell viability (%) was calculated using the formula 2 mentioned above in subsection "2.5.1".

## 2.7. Statistical analysis

The collected data underwent statistical analysis using SPSS version 18 (SPSS Inc., Chicago, IL, USA). The initial step involved an analysis of variance (ANOVA) for comparing multiple samples, followed by Tukey's multiple comparison test.

## 3. Results and discussion

### 3.1. BAu/Ag-nanoalloy synthesis and ginger aqueous-extract analysis

In comparison to alternative biological synthesis methods involving microbes, there are several advantages to synthesizing nanoalloys utilizing plant extracts. This finding is due to cost-effectiveness, avoidance of contaminants, faster method, single-step, handling safe, enhanced nanoparticle stability due to massive metabolite secretion, suitability for commercial production, eco-friendly approach, and low Lab requirements for nanoparticle synthesis (Ghosh et al., 2023). In addition to the primary function of plant secondary metabolites (i.e., phenols, carbohydrates, proteins, flavonoids, steroids, alkaloids, tannins, sugars, and terpenoids) in the reduction and stabilizing nanoparticles, it can impart additional functions such as antimicrobial and antiviral to the newly synthesized materials. Therefore, this phenomenon can produce various nanoparticles (either in a single form or as bimetallic) for biomedical applications. The current study fabricated BAu/Ag nanoalloy using a ginger rhizome extract. This fabrication is due to the activity of metabolites in the ginger extract to reduce the HAuCl<sub>4</sub> and AgNO<sub>3</sub> and form nanoalloys, followed by the capping and stabilization of the formed nanoparticles.

Au-NPs and Ag-NPs were also synthesized using ginger aqueous extract utilizing the activity of metabolites that act as reducing/capping agents for as-prepared nanoparticles (Yadi et al., 2022). Also, Au-, Ag-, and bimetallic Au/Ag-NPs were fabricated using leaf aqueous extract of *Piper pedicellatum* (Tamuly et al., 2013). The authors reported that the successful formation of these nanoparticles could be attributed to the active metabolites that exist in plant aqueous extract in reduction-, capping-, and stabilizing- nanomaterials. In this study, the ginger rhizome's main components (carbohydrates, proteins, and phenols) were determined quantitatively. The analysis showed that the rhizome of ginger contained 37.3 mg·g<sup>-1</sup>, 0.75 mg·g<sup>-1</sup>, and 0.03 mg·g<sup>-1</sup> of total soluble carbohydrates, total soluble proteins, and total phenolic compounds, respectively.

### 3.2. Characterization

#### 3.2.1. *UV-vis spectroscopy*

Shifting the plant's aqueous extract color from pale yellow to reddish-purple after mixing with  $\text{HAuCl}_4$  and  $\text{AgNO}_3$  is considered the first sign of BAu/Ag-NPs synthesis. This shifting confirmed the activity of metabolites to form nanoscale structures by metal ions reduction. The absorbance of the new color was measured at 200–800 nm to detect the maximum SPR. Two maximum SPR were observed at wavelengths of 440 and 545 nm, which corresponded to Ag and Au absorbance, respectively (Fig. 1). In a similar study, the Au-Ag nanoparticles (with 1:1 ratio) that formed using leaf aqueous extract of *Anacardium occidentale* showed absorbance bands at wavelengths of 502 and 413 nm, which corresponded to the SPR of Au and Ag, respectively (Sheny et al., 2011). In contrast, two peaks at 350 and 544 nm were observed in the UV spectrum of Au-NPs synthesized by bacterial strain *E.coli*, whereas one peak was observed at 360 nm for Au/Ag-NPs spectrum (Jiang et al., 2019).

#### 3.2.2. *FT-IR spectroscopy*

The biosynthesized BAu/Ag-NPs and the aqueous extract's chemical composition were determined using the FT-IR. Five individual peaks were seen by the FT-IR chart of the plant extract at the following wavenumbers: 3440, 2072, 1632, 1410, and 1047  $\text{cm}^{-1}$ . When interacting with bimetallic gold and silver to generate BAu/Ag-NPs, the positions of these peaks changed, and new peaks appeared (Fig. 2, Table 1). Various groups related to different molecules, including proteins, amino acids, amines, and polysaccharides, are present in the ginger extracts. The observed peaks in FT-IR spectra at wavenumbers 3440, 1632, and 1410  $\text{cm}^{-1}$  were shifted to 3421, 1619, and 1422  $\text{cm}^{-1}$ , respectively. The peak at 2072  $\text{cm}^{-1}$  disappeared after the fabrication of BAu/Ag-NPs, whereas new peaks at 2931, 1382, 878, 775, and 610  $\text{cm}^{-1}$  appeared on the FT-IR chart of nanoalloy. The results are consistent with various studies on bimetallic nanoparticle fabrications using plant aqueous extract (Sheny et al., 2011). Appearance or disappearance and changes in the position of their respective spectral bands demonstrate that these groups can reduce, capping, and stabilize the newly produced BAu/Ag-NPs. The explanation of different peaks in FT-IR spectra is discussed in Table 1.

#### 3.2.3. *Morphological and elemental analysis*

TEM is an important tool for analyzing the shape/size of

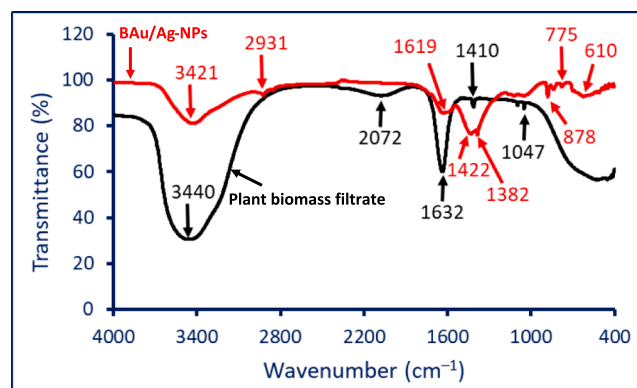


Fig. 2. FT-IR analysis of ginger aqueous extract and biosynthesized BAu/Ag-NPs.

Table 1

Peaks of FT-IR analysis of plant aqueous extract and the biosynthesized BAu/Ag-NPs.

Vibration	Plant aqueous extract	BAu/Ag nanoalloy	References
Stretching OH/NH overlapped	3440	3421	(Hamza et al., 2022a)
Stretching CH of aliphatic hydrocarbons		2931	(Fouda et al., 2022a)
Aromatic compounds exhibited overlapping with the $\nu(\text{C-O})$ vibration	2072	–	(Khademi-Azandehi and Moghaddam, 2015)
The stretching of C = O, C = N vibrations amides, and N–H in primary amines (overlapped)	1632	619	(Sheny et al., 2011)
The stretching N–H and O–H in secondary amines overlap with the binding C–H	1410	1422, 1382	(Ghosh et al., 2023)
Stretching CN	1047	–	(Lawrie et al., 2007)
Aromatic CH in-plane bend	–	878	(Hamza et al., 2022b)
Bending CH of plane	–	775, 610	(Coates, 2000)

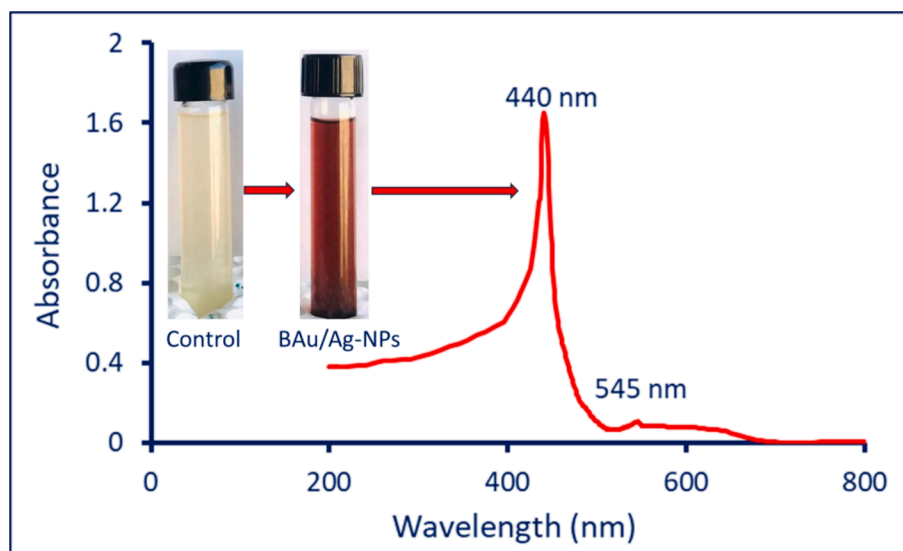


Fig. 1. The detection of maximum SPR of green synthesized BAu/Ag-NPs by UV-Vis spectroscopy, in addition to the digital photo for plant aqueous extract and reddish purple color formed due to fabrication of BAu/Ag-NPs.

nanoparticles in nanotechnology and materials science. In this context, bimetallic Au/Ag nanoparticles were synthesized using a ginger aqueous extract, and their size, shape, and distribution were analyzed using TEM. Herein, the synthesized bimetallic nanoalloy exhibited spherical shapes with a size range of 10–100 nm at an average size of  $49.1 \pm 16.2$  nm (Fig. 3A and B). TEM analysis is crucial in investigating the BAu/Ag-NPs size and shape. Firstly, it gives us a chance to examine the morphological characteristics of nanoparticles, proving beyond a reasonable doubt that they have a spherical shape. This is helpful because nanoparticle shapes affect their characteristics and potential uses. For instance, spherical nanoparticles are ideal for various applications due to their uniform characteristics and low scattering, making them useful in fields as diverse as catalysis, drug delivery, and imaging (Altammar, 2023). The activity of nanoparticles to suppress the growth of *P. aeruginosa*, *E. coli*, and *S. aureus* was shape-dependent, as reported previously (Cheon et al., 2019). The authors found that spherical nanoparticles had the most antibacterial activity compared to disc and triangle shapes.

Secondly, TEM gives accurate size data, and our results showed that BAu/Ag-NPs of an average size of  $49.1 \pm 16.2$  nm. This data is crucial because nanoparticle size can impact their optical, electrical, catalytic, and biomedical properties. Therefore, it can modify the properties of nanoparticles for particular uses by controlling their size due to their direct effects on the diffusion and distribution of nanoparticles.

Interestingly, the exponential rise in the surface area is associated with the decrease in particle size. Therefore, smaller nanoparticles are more reactive in biological environments. For instance, the sizes in the ranges of 10–16 nm Au-NPs can be accumulated in the cytoplasm, whereas the smaller sized (6 nm) can enter the nucleus. Hence, the authors concluded that the smaller sizes were more toxic (Huo et al., 2014).

The TEM study also showed that the BAu/Ag-NPs were uniformly scattered. Aggregation or agglomeration of nanoparticles can significantly alter their behavior and function hence this finding is critical. In many contexts, well-dispersed nanoparticles are more reliable and stable. Based on the above discussion, the spherical shape, well-defined size range, and well-dispersed bimetallic Au/Ag-NPs synthesized with ginger aqueous extract provide a promising foundation for further exploration in areas such as medications, pharmaceuticals, biomedical, catalysis, drug delivery, and beyond.

Following TEM analysis, the elementary mapping of the bimetallic Au/Ag-NPs was determined using EDX analysis. The obtained data revealed that the as-formed sample predominantly contains Au and Ag ions, as indicated by their percentages of weight (28.6 and 45.9 %) and atomic (31.2 and 47.1 %), respectively (Fig. 3B). Specifically, the presence of signals at bending energies of 1.8, 2.12, and 9.8 KeV corresponds to Au, whereas peaks at 2.9, 3.1, 3.3, and 3.5 KeV are characteristics of Ag. Our results were compatible with previous studies

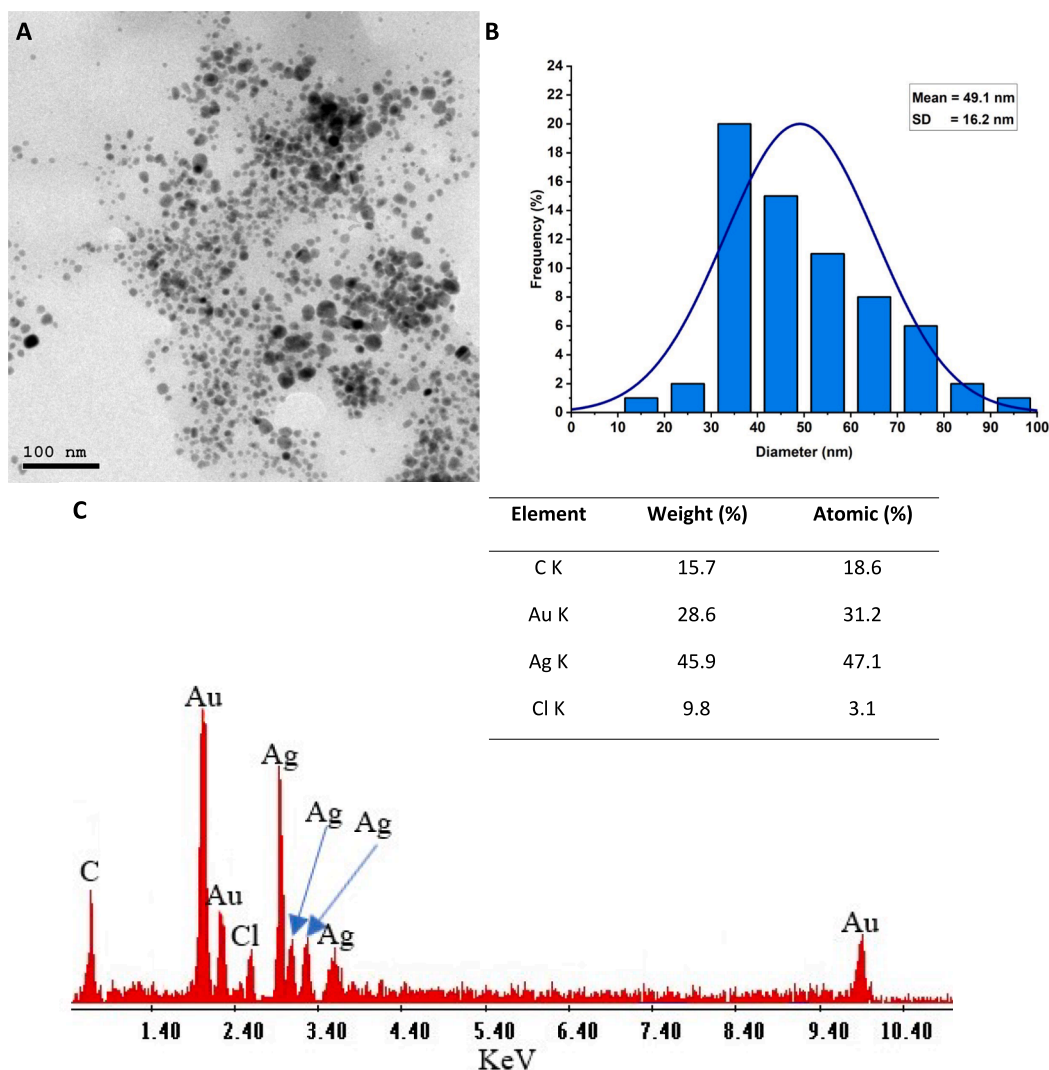


Fig. 3. (A) Transmission electron microscopy analysis showed spherical shape, well-defined sizes, and well-arranged BAu/Ag nanoalloy, (B) Size distribution graph based on the calculation of a wide range of sizes from TEM image, (C) Energy-dispersive X-ray (EDX) analysis reveals the chemical components of nanoalloy.

dealing with the synthesis of Au/Ag-NPs using either plant or microbial extracts and chemical methods (Sheny et al., 2011, Sahu et al., 2020). The existence of C and Cl peaks may be related to the scattering of the capping agent from the plant extract that coated nanoparticles for stabilization (Fouda et al., 2023). EDX analysis is helpful because it confirms the presence and distribution of the desired metals inside the bimetallic structure by revealing insights into the elemental composition of a nanostructure. Knowing the NP's elemental composition is essential for designing materials with the appropriate qualities and determining which ones may be used in a particular application.

### 3.2.4. XRD analysis

The XRD was utilized to analyze the crystallinity structure of BAu/Ag nanoalloys. As shown, the XRD chart of BAu/Ag-NPs showed five intense reflection peaks at  $2\theta$  of  $38.2^\circ$ ,  $44.3^\circ$ ,  $64.3^\circ$ ,  $77.3^\circ$ , and  $85.6^\circ$ , which signify the Bragg diffraction of (1 1 1), (200), (220), (311), and (222) respectively (Fig. 4). In a recent investigation, the XRD of monometallic Au-NPs formed by ginger aqueous extract showed four reflection signals at Bragg diffraction of (1 1 1), (200), (220), and (311) related to planes of  $38.2^\circ$ ,  $44.5^\circ$ ,  $64.8^\circ$ , and  $77.7^\circ$  respectively (Fouda et al., 2022). These data confirmed the face-centered cubic (FCC) structure of BAu/Ag-NPs, as shown in monometallic Au-NPs. The obtained data are similar to the results of Gupta et al. (Gupta et al., 2020). The authors successfully synthesized monometallic (Au-NPs, Ag-NPs), and bimetallic (Au/Ag) nanoalloys using an aqueous extract of *Moringa oleifera* leaves. In the XRD analysis of the obtained nanoparticles, they observed distinct diffraction peaks at specific angles: ( $38.2^\circ$ ,  $46.2^\circ$ ,  $64.6^\circ$ , and  $77.3^\circ$ ) for Ag ( $38.22^\circ$ ,  $44.38^\circ$ ,  $64.89^\circ$ ,  $77.49^\circ$ , and  $81.81^\circ$ ) for Au, and ( $38.18^\circ$ ,  $46.29^\circ$ ,  $64.71^\circ$ ,  $76.69^\circ$ , and  $85.68^\circ$ ) for bimetallic Au/Ag-NPs. These peaks corresponded to specific crystallographic planes, including (1 1 1), (200), (220), (311), and (222). Notably, these peaks in bimetallic Au/Ag-NPs confirmed their crystalline structure. This confirmation was based on the observation that the bimetallic nanoparticles exhibited the same peaks as those in monometallic Ag and Au-NPs. Similarly, the XRD pattern of Au-NPs revealed distinct peaks at four specific angles with  $2\theta$  of  $38.2^\circ$ ,  $44.5^\circ$ ,  $64.7^\circ$ , and  $77.8^\circ$ , corresponding to crystallographic planes (1 1 1), (200), (220), and (311), respectively. Interestingly, the fabricated bimetallic Au/Ag-NPs exhibited identical planes with diffraction peaks at  $38.1^\circ$ ,  $44.3^\circ$ ,  $64.5^\circ$ , and  $77.3^\circ$ . This observation confirmed that both the monometallic and bimetallic nanoparticles possessed an FCC crystal structure (Berahim et al., 2018). From the XRD pattern, the average crystallite size of BAu/Ag nanoalloys was determined to be 39 nm using Scherrer's equation.

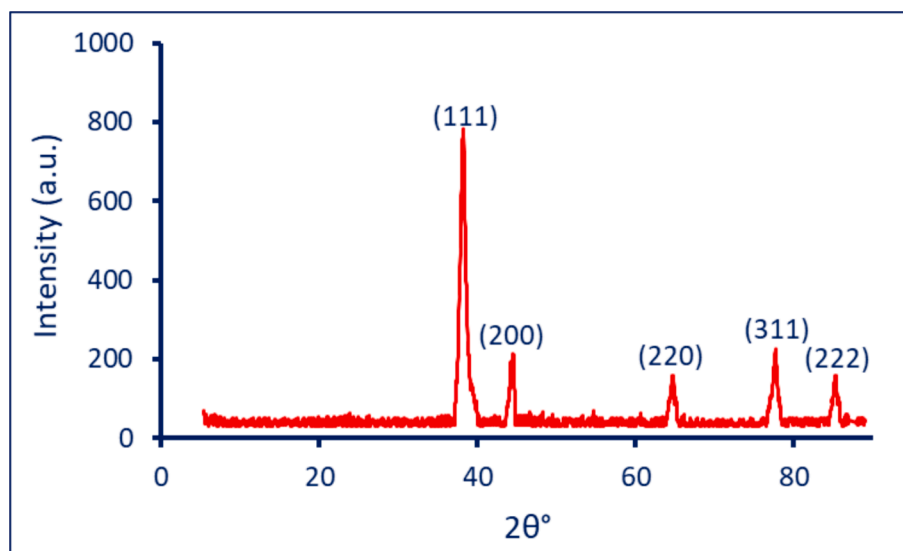


Fig. 4. The crystallographic assessment of BAu/Ag-NPs was fabricated ginger aqueous extract.

### 3.3. Antiviral activity

The cytotoxicity effect of synthesized BAu/Ag-NPs on Vero normal cells was achieved before assessing their antiviral activity. The goal was to ensure that the BAu/Ag-NPs had antiviral effects against viruses while simultaneously causing the minor damage possible to the host cells. The cytotoxicity of the BAu/Ag-nanoalloy-treated Vero cells was determined, and the half cytotoxic concentration ( $CC_{50}$ ) was about  $207.74 \mu\text{g}\cdot\text{mL}^{-1}$ . The cytotoxicity manifested as a reduced cellular growth rate, leading to cell rounding, surface detachment, and clumping. When the BAu/Ag-NPs concentration decreased to  $125 \mu\text{g}\cdot\text{mL}^{-1}$ , no toxicity was observed in Vero cells (Fig. 5). This concentration was consequently considered as the maximum non-toxic concentration (MNTC) for evaluating their antiviral activity.

The results showed an increased Vero cell viability treated with HAV and Cox-B4 from 47.13 % and 37.3 % to 88.5 % and 80.9 %, respectively, after being treated with BAu/Ag-NPs (Table 2). The results showed that the phytosynthesized nanoalloy Au/Ag has antiviral activity with percentages of 78.2 % and 69.6 % for HAV and Cox-B4, respectively (Table 2).

The multifaceted antiviral effects of BAu/Ag-NPs synthesized from ginger rhizome aqueous extract against HAV and Cox-B4 are due to varied mechanisms, including their ability to prevent viral attachment and entry, interfere with viral replication, induce oxidative stress,

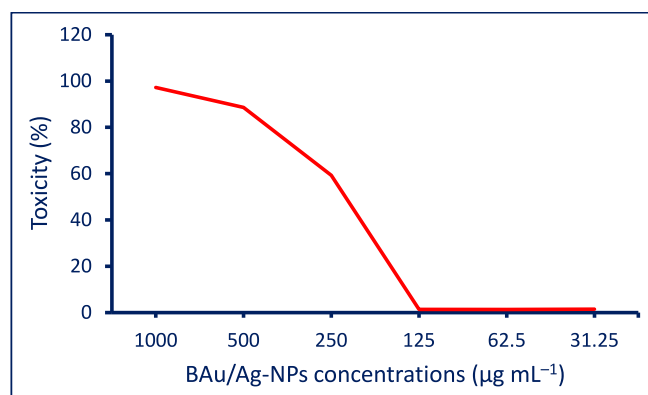


Fig. 5. Toxicity assessment of the biofabricated BAu/Ag-NPs against normal Vero cell lines.

**Table 2**

Antiviral assessment for the sublethal concentration of BAu/Ag-NPs at the MNTC of 125  $\mu\text{g.mL}^{-1}$  against HAV and Cox-B4 viruses.

Treatment	Cell viability	Cell toxicity	Viral activity	Antiviral effect
Control (Vero normal cell)	100 $\pm$ 0.0 %	0	0	0
Vero cell + HAV	47.13 $\pm$ 0.4 %	52.9 $\pm$ 0.8	100 $\pm$ 0.0 %	0
Vero cell + HAV + BAu/Ag-NPs	88.5 $\pm$ 0.5 %	11.5 $\pm$ 0.6 %	21.8 $\pm$ 1.5 %	78.2 $\pm$ 0.8 %
Vero cell + Cox-B4	37.3 $\pm$ 0.5 %	62.7 $\pm$ 1.1 %	100 $\pm$ 0.0 %	0
Vero cell + Cox-B4 + BAu/Ag-NPs	80.9 $\pm$ 0.6 %	19.1 $\pm$ 0.6 %	30.4 $\pm$ 1.2 %	69.6 $\pm$ 0.6 %

modulate the host immune response, prevent apoptosis, reduce viral load, and possibly benefit from synergy between gold and silver components. BAu/Ag-NPs can prevent virus attachment to host cells by interacting with the viral envelope or surface proteins. This block is due to the ability of viruses like HAV and Cox-B4 to enter host cells by interacting with receptors on the cell membrane. To make more virus particles, viruses must multiply inside the host cell. Bimetallic nanoparticles have been shown to disrupt the viral replication process in many steps. They could interfere with replication by damaging viral RNA or DNA or blocking viral enzymes vital to the replication process (Louten, 2016).

Moreover, the infected cells may produce reactive oxygen species (ROS) against bimetallic NPs. Damage to viral DNA, proteins, and lipid membranes can result from elevated amounts of ROS. The virus' ability to replicate and infect cells can be compromised by oxidative damage. Au/Ag-NPs may also modulate the host immune response. They can enhance the host's ability to recognize and respond to viral infections by stimulating the production of immune cells and molecules, such as interferons and proinflammatory cytokines. This heightened immune response aids in the elimination of infected cells and controls viral spread. To escape from infected cells, viruses frequently trigger their death through apoptosis. By preventing the activation of apoptotic pathways, bimetallic nanoparticles can suppress apoptosis. As a result, infected cells are spared death, giving the immune system additional time to eradicate the pathogen. Also, the coating of the surface of the bimetallic nanoparticles by active compounds from ginger extract can enhance their stability and biocompatibility, ensuring efficient delivery to the target cells. Finally, synergistic actions between the Au and Ag in the fabricated bimetallic NPs may increase their potency against viruses. Gold's presence can increase stability and improve interaction with biomolecules in silver nanoparticles (Rabiee et al., 2022). These multifaceted mechanisms collectively contribute to the antiviral properties of BAu/Ag-NPs.

### 3.4. Anticancer

An important step forward in medicine is the introduction of nanoparticles, particularly in diagnosing and treating cancer. Nanoparticles can revolutionize cancer treatment due to the unique properties of nanoparticles compared to bulk (precursor) materials. Their size allows them to precisely target cancer cells without harming healthy tissue. With this tailored strategy, cancer therapies like chemotherapy and radiation cause much less collateral harm and side effects. Nanoparticles can also deliver drugs directly to cancer cells, improving bioavailability and efficacy. The increased surface area/volume ratio allows medication loading and regulated release for sustained therapeutic impact. Diagnostic and therapeutic skills merge to create a new age in customized medicine, enabling tailored treatment regimens and better patient results.

The MTT assay is essential in cancer research for quickly evaluating

cell toxicity, including the effects of nanoparticles. It helps find the best nanoparticle concentrations for treatment while minimizing side effects. Herein, the effect of biosynthesized BAu/Ag-NPs against oral normal epithelial cell lines (OEC), adenocarcinoma cell lines (MCF7), and hepatocarcinoma cell lines (HepG2) was investigated using MTT assay method (Fig. 6). Data analysis reveals the cytotoxicity of bimetallic nanoalloy against normal and cancer cells was concentrations-dependent. This result was compatible with studies dealing with the in-vitro cytotoxic effect of nanoparticles against different cell lines (Gupta et al., 2020, Fouda et al., 2022). As shown, the cell lines (MCF7, HepG2, and OEC) lost about 96 %, 95 %, and 46 % of their viability, respectively, after being treated with 500  $\mu\text{g.mL}^{-1}$  of BAu/Ag-NPs (Fig. 6). In a recent study, the viability of the same cancer and normal cells, MCF7, HepG2, and OEC, were decreased with percentages of 70 %, 94 %, and 50 %, respectively, after treatment with 500  $\mu\text{g.mL}^{-1}$  of monometallic Au-NPs fabricated by ginger rhizome extract (Fouda et al., 2022b). This indicated that the anticancer activity of the BAu/Ag-nanoalloy was more active compared to monometallic NPs. At 250  $\mu\text{g.mL}^{-1}$ , cancer and normal cell lines viability were recovered at 39.5  $\pm$  0.7 %, 22.5  $\pm$  0.7 %, and 99.5  $\pm$  1.4 % for MCF7, HepG2, and OEC, respectively (Fig. 6). This indicated that HepG2 hepatocarcinoma cells are a more amenable target for BAu/Ag-NPs generated using ginger rhizome-mediated techniques than MCF7 adenocarcinoma cells. Moreover, at 250  $\mu\text{g.mL}^{-1}$  and below, the negative impact of nanoalloy on normal oral epithelial cells was minimal or neglected.

Half-maximal inhibitory concentration ( $\text{IC}_{50}$ ) of BAu/Ag-NPs is crucial for assessing their efficacy, safety, and potential as therapeutic agents. This data plays a pivotal role in precision medicine, quality control, regulatory compliance, and the development of innovative NP-based treatments. In this study, the  $\text{IC}_{50}$  of phytosynthesized BAu/Ag-NPs was 502.5  $\pm$  2.8, 212.6  $\pm$  4.4, and 117.9  $\pm$  6.6  $\mu\text{g mL}^{-1}$  for normal OEC, cancerous MCF7, and HepG2 respectively. In a similar study, the  $\text{IC}_{50}$  values of monometallic (Ag- and Au-) and bimetallic (Au/Ag)- NPs fabricated by *Moringa oleifera* aqueous leaves-extract were (92.2  $\pm$  2.2, 19.02  $\pm$  4.5, and 37.2  $\pm$  2.6  $\mu\text{g.mL}^{-1}$ ), (128.3  $\pm$  1.8, 21.5  $\pm$  1.4, and 49.9  $\pm$  0.2  $\mu\text{g.mL}^{-1}$ ), and (821.01  $\pm$  2.8, 9.2  $\pm$  0.9, and 45.6  $\pm$  0.2  $\mu\text{g.mL}^{-1}$ ) for HepG2, MDA-MB-231, and MCF7, respectively (Gupta et al., 2020). The variation in the cytotoxic efficacy of mono and bimetallic nanoparticles could be attributed to the synthesis approach either using plant extract, microbial extract, chemical, or physical methods. The low cytotoxicity of ginger-mediated BAu/Ag-NPs on normal cell lines compared to the high toxicity toward cancer cell lines like HepG2 and MCF7 can be attributed to a selective targeting of cancer cells. This selectivity may be explained by several variables, such as how cancer and normal cells absorb substances differently, how those substances are processed inside cells, and how sensitive they are to cytotoxic effects. Besides that, the physico-chemical properties of the NPs, such as size, shape, and surface functionalization contributed to their preferential targeting of cancer cells while sparing normal cells.

The anticancer property of bimetallic nanoparticles depends on the nature, concentrations, and synergistic effects of the metals in their composition. Herein, the combination of Au and Ag may result in synergistic effects that improve and enhance their anticancer activity, especially in cases where both Au and Ag have high cytotoxic effects. The effect of bimetallic Ag/Au nanoalloy on the lung carcinoma cells exhibiting the interaction of the metals could be attributed to the topological distribution of metals within the bimetallic nanoparticles (Shmarakov et al., 2017). Moreover, the cytotoxicity of BAu/Ag-NPs could be due to the varied cellular uptake between cancer and normal cells. In most cases, cancer cells have a high endocytosis rate and, hence, are more susceptible to nanoparticle uptake.

The potential anticancer mechanism for nanoparticles, notably Ag and Au, could be related to the oxidative stress induced by the generation of ROS upon the entrance of nanoparticles into the cells and reaction with biological macromolecules. The increased ROS damages cellular components (e.g. proteins, nucleic acids, lipids, mitochondria,

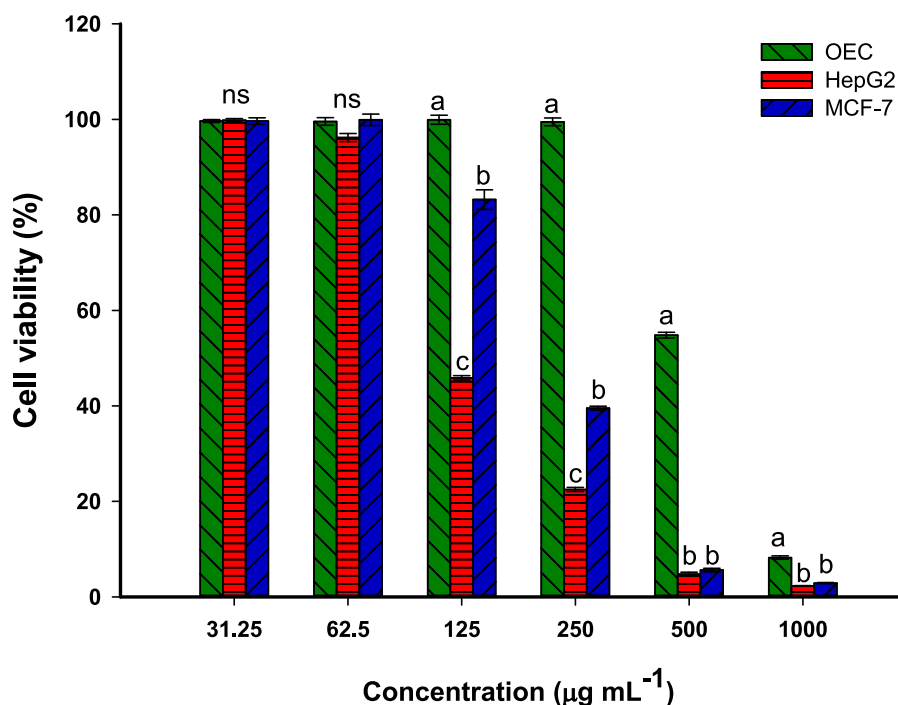


Fig. 6. *In-vitro* cytotoxicity of the phytosynthesized BAu/Ag-NPs against normal (OEC) and cancer cell lines (HepG2 and MCF7).

and other essential micro- and macromolecules), ultimately leading to cell death. In addition, the NPs might interfere with signaling pathways needed for the survival and proliferation of cancer cells. The NPs can inhibit the enzymes and proteins regulating cellular processes for cancer cell growth and survival. Another anticancer mechanism of nanoparticles is apoptosis, defined as programmed cell death. This mechanism is essential to turnover and eliminate the damaged or abnormal cells, including cancer cells. Some nanoparticles, including Ag and Au, can induce cancer cell death by inhibiting the anti-apoptotic proteins or activating apoptotic pathways (Pistrutto et al., 2016). Also, endocytosis is a mechanism used to uptake nanoparticles inside the cells, leading to their accumulation within different cellular components. As a result, the nanoparticles interact with various organelles, leading to dysfunction and elevate the cytotoxic effects (Ibrahim et al., 2022). Finally, some nanoparticles have an immunomodulatory character that affects the immune response toward cancer cells, leading to the suppression or elimination of these abnormal cells.

#### 4. Conclusion

In the current investigation, the aqueous extract of ginger rhizome was used for the biofabrication of bimetallic Au/Ag-NPs. Using comprehensive characterization tools, including UV-Vis, FT-IR, TEM, EDX, and XRD analyses, we confirm a spherical shape with an average size of 49.1 nm and crystalline nanoalloys. Moreover, the synthesized nanoalloy contains Au and Ag, which have the highest weight and atomic percentages. These nanoalloys exhibited significant antiviral activity against HAV (78.2 %) and Cox-B4 (69.6 %) viruses. Furthermore, they displayed selective cytotoxicity towards cancer cell lines (MCF7 and HepG2) while demonstrating low toxicity to normal oral epithelial cells (IC<sub>50</sub>: 502.5 ± 2.8 µg·mL<sup>-1</sup>). The study's results highlight the adaptability and efficacy of green synthesis methods and pave the way for future research into the biomedical applications of bimetallic nanoalloys. More research is required into their molecular effects, in-vivo trials, and clinical applications to realize their potential as therapeutic agents fully.

#### Funding

This work received no external funding.

#### CRediT authorship contribution statement

**Khalid S. Alshallash:** Validation, Resources, Project administration, Funding acquisition, Formal analysis. **Ahmed M. Eid:** . **Saad El-Din Hassan:** Writing – review & editing, Supervision, Software, Project administration, Investigation, Formal analysis, Conceptualization. **Mohammed Ali Abdel-Rahman:** Writing – original draft, Validation, Supervision, Investigation, Formal analysis, Conceptualization. **Abdullah S. Alawam:** Validation, Resources, Project administration, Funding acquisition, Data curation. **Mohammed F. Hamza:** Writing – review & editing, Visualization, Software, Methodology, Formal analysis, Conceptualization. **Amr Fouda:** Writing – review & editing, Writing – original draft, Validation, Supervision, Project administration, Methodology, Formal analysis, Data curation, Conceptualization.

#### Acknowledgments

The authors extend their appreciation to the Botany and Microbiology Department, Faculty of Science, Al-Azhar University, Cairo, Egypt, for the great support in the achievement and publication of this research work. Furthermore, the authors acknowledge the support from Imam Mohammad Ibn Saud Islamic University Riyadh, Saudi Arabia.

#### References

- Abdel-Rahman, M.A., Alshallash, K.S., Eid, A.M., et al., 2024. Exploring the Antimicrobial, Antioxidant, and Antiviral Potential of Eco-Friendly Synthesized Silver Nanoparticles Using Leaf Aqueous Extract of *Portulaca oleracea* L. *Journal* 17 (3). <https://doi.org/10.3390/ph17030317>.
- Ainsworth, E.A., Gillespie, K.M., 2007. Estimation of total phenolic content and other oxidation substrates in plant tissues using Folin-Ciocalteu reagent. *Nat. Protoc.* 2 (4), 875–877. <https://doi.org/10.1038/nprot.2007.102>.
- Altammar, K.A., 2023. A review on nanoparticles: characteristics, synthesis, applications, and challenges. *Front. Microbiol.* 14, 1155622. <https://doi.org/10.3389/fmicb.2023.1155622>.

- Amin, M.A., Ismail, M.A., Badawy, A.A., et al., 2021. The Potency of Fungal-Fabricated Selenium Nanoparticles to Improve the Growth Performance of *Helianthus annuus* L. and Control of Cutworm *Agrotis ipsilon*. *Journal* 11 (12). <https://doi.org/10.3390/catal11121551>.
- Berahim, N., Basirun, W.J., Leo, B.F., et al., 2018. Synthesis of Bimetallic Gold-Silver (Au-Ag) Nanoparticles for the Catalytic Reduction of 4-Nitrophenol to 4-Aminophenol. *Journal* 8 (10). <https://doi.org/10.3390/catal8100412>.
- Cheon, J.Y., Kim, S.J., Rhee, Y.H., et al., 2019. Shape-dependent antimicrobial activities of silver nanoparticles. *Int. J. Nanomed.* 14, 2773–2780. <https://doi.org/10.2147/ijn.s196472>.
- Coates, J., 2000. Interpretation of infrared spectra, a practical approach. In *Encyclopedia of Analytical Chemistry*; John Wiley & Sons Ltd.: Hoboken, NJ, USA.
- Eid, A.M., Fouda, A., Hassan, S.E., et al., 2023. Plant-Based Copper Oxide Nanoparticles; Biosynthesis, Characterization, Antibacterial Activity, Tanning Wastewater Treatment, and Heavy Metals Sorption. *Journal* 13 (2). <https://doi.org/10.3390/catal13020348>.
- Fouda, A., Eid, A.M., Abdel-Rahman, M.A., et al., 2022a. Enhanced Antimicrobial, Cytotoxicity, Larvicidal, and Repellence Activities of Brown Algae, *Cystoseira crinita*-Mediated Green Synthesis of Magnesium Oxide Nanoparticles. *Front. Bioeng. Biotechnol.* 10, 849921 <https://doi.org/10.3389/fbioe.2022.849921>.
- Fouda, A., Eid, A.M., Guibal, E., et al., 2022b. Green Synthesis of Gold Nanoparticles by Aqueous Extract of *Zingiber officinale*: Characterization and Insight into Antimicrobial, Antioxidant, and In Vitro Cytotoxic Activities. *Appl. Sci.* 12 (24), 12879.
- Fouda, A., Alshallash, K.S., Alghonaim, M.I., et al., 2023. The Antimicrobial and Mosquitocidal Activity of Green Magnesium Oxide Nanoparticles Synthesized by an Aqueous Peel Extract of *Punica granatum*. *Journal* 5 (3), 2009–2024. <https://doi.org/10.3390/chemistry5030136>.
- M. Ghasemi T. Turnbull S. Sebastian et al. The MTT Assay: Utility, Limitations, Pitfalls, and Interpretation in Bulk and Single-Cell Analysis. *International Journal of Molecular Sciences.* 22 23 2021 10.3390/ijms222312827.
- Ghosh, S., Roy, S., Naskar, J., et al., 2023. Plant-Mediated Synthesis of Mono- and Bimetallic (Au–Ag) Nanoparticles: Future Prospects for Food Quality and Safety. *J. Nanomater.* 2023, 2781667. <https://doi.org/10.1155/2023/2781667>.
- Gupta, S., Hemlata, H., Tejavath, K., 2020. Synthesis, characterization and comparative anticancer potential of phytosynthesized mono and bimetallic nanoparticles using *Moringa oleifera* aqueous leaf extract. *Beilstein Arch.* 1, 95.
- Hamza, M.F., Fouda, A., Wei, Y., et al., 2022a. Functionalized biobased composite for metal decontamination – Insight on uranium and application to water samples collected from wells in mining areas (Sinai, Egypt). *Chem. Eng. J.* 431, 133967 <https://doi.org/10.1016/j.cej.2021.133967>.
- Hamza, M.F., Hamad, D.M., Hamad, N.A., et al., 2022b. Functionalization of magnetic chitosan microparticles for high-performance removal of chromate from aqueous solutions and tannery effluent. *Chem. Eng. J.* 428, 131775 <https://doi.org/10.1016/j.cej.2021.131775>.
- Han, H.S., Choi, K.Y., 2021. Advances in Nanomaterial-Mediated Photothermal Cancer Therapies. Toward Clinical Applications. *Biomedicines.* 9 (3) <https://doi.org/10.3390/biomedicines9030305>.
- Hu, D., Gao, T., Kong, X., et al., 2022. Ginger (*Zingiber officinale*) extract mediated green synthesis of silver nanoparticles and evaluation of their antioxidant activity and potential catalytic reduction activities with Direct Blue 15 or Direct Orange 26. *PLoS One.* 17 (8), e0271408.
- Huo, S., Jin, S., Ma, X., et al., 2014. Ultrasmall Gold Nanoparticles as Carriers for Nucleus-Based Gene Therapy Due to Size-Dependent Nuclear Entry. *ACS Nano* 8 (6), 5852–5862. <https://doi.org/10.1021/nn5008572>.
- Ibrahim, A.G., Fouda, A., Elgammal, W.E., et al., 2022. New thiadiazole modified chitosan derivative to control the growth of human pathogenic microbes and cancer cell lines. *Sci. Rep.* 12 (1), 21423. <https://doi.org/10.1038/s41598-022-25772-4>.
- Jiang, X., Fan, X., Xu, W., et al., 2019. Biosynthesis of bimetallic Au–Ag nanoparticles using *Escherichia coli* and its biomedical applications. *ACS Biomater. Sci. Eng.* 6 (1), 680–689.
- Khademi-Azandehi, P., Moghaddam, J., 2015. Green synthesis, characterization and physiological stability of gold nanoparticles from *Stachys lavandulifolia* Vahl extract. *Particuology.* 19, 22–26. <https://doi.org/10.1016/j.partic.2014.04.007>.
- Lawrie, G., Keen, I., Drew, B., et al., 2007. Interactions between Alginate and Chitosan Biopolymers Characterized Using FTIR and XPS. *Biomacromolecules.* 8 (8), 2533–2541. <https://doi.org/10.1021/bm070014y>.
- Louten, J., 2016. Virus replication. *Essential Human Virology.* 49–70.
- Makada, H., Habib, S., Singh, M., 2023. Bimetallic nanoparticles as suitable nanocarriers in cancer therapy. *Scientific African.* 20, e01700.
- Malik, S., Muhammad, K., Waheed, Y., 2023. Nanotechnology: A Revolution in Modern Industry 28. <https://doi.org/10.3390/molecules28020661>.
- Mao, Q.Q., Xu, X.Y., Cao, S.Y., et al., 2019. Bioactive Compounds and Bioactivities of Ginger (*Zingiber officinale* Roscoe). *Foods (Basel, Switzerland)* 8 (6). <https://doi.org/10.3390/foods8060185>.
- Nassar, A.-R.-A., Atta, H.M., Abdel-Rahman, M.A., et al., 2023. Myco-synthesized copper oxide nanoparticles using harnessing metabolites of endophytic fungal strain *Aspergillus terreus*: an insight into antibacterial, anti-*Candida*, biocompatibility, anticancer, and antioxidant activities. *BMC Complementary Medicine and Therapies.* 23 (1), 261. <https://doi.org/10.1186/s12906-023-04056-y>.
- Pistritto, G., Trisciuglio, D., Ceci, C., et al., 2016. Apoptosis as anticancer mechanism: function and dysfunction of its modulators and targeted therapeutic strategies. *Aging.* 8 (4), 603–619. <https://doi.org/10.18632/aging.100934>.
- Rabiee, N., Ahmadi, S., Akhavan, O., et al., 2022. Silver and Gold Nanoparticles for Antimicrobial Purposes against Multi-Drug Resistance Bacteria. *Materials (basel, Switzerland)* 15 (5). <https://doi.org/10.3390/ma15051799>.
- Sahu, S., Sharma, S., Ghosh, K.K., 2020. Novel formation of Au/Ag bimetallic nanoparticles from a mixture of monometallic nanoparticles and their application for the rapid detection of lead in onion samples. *New J. Chem.* 44 (35), 15010–15017. <https://doi.org/10.1039/D0NJ02994G>.
- Salem, S.S., El-Belely, E.F., Niedbala, G., et al., 2020. Bactericidal and In-Vitro Cytotoxic Efficacy of Silver Nanoparticles (Ag-NPs) Fabricated by Endophytic Actinomycetes and Their Use as Coating for the Textile Fabrics. *Journal* 10 (10). <https://doi.org/10.3390/nano10102082>.
- Sheny, D.S., Mathew, J., Philip, D., 2011. Phytosynthesis of Au, Ag and Au–Ag bimetallic nanoparticles using aqueous extract and dried leaf of *Anacardium occidentale*. *Spectrochimica Acta Part a: Molecular and Biomolecular Spectroscopy.* 79 (1), 254–262. <https://doi.org/10.1016/j.saa.2011.02.051>.
- Shmarakov, I., Mukha, I., Vityuk, N., et al., 2017. Antitumor activity of alloy and core-shell-type bimetallic AgAu nanoparticles. *Nanoscale Res. Lett.* 12, 1–10.
- Singh, C., Mehata, A.K., Priya, V., et al., 2022. Bimetallic Au-Ag Nanoparticles: Advanced Nanotechnology for Tackling Antimicrobial Resistance. *Molecules (Basel, Switzerland)* 27 (20). <https://doi.org/10.3390/molecules27207059>.
- Tamuly, C., Hazarika, M., Borah, S., et al., 2013. In situ biosynthesis of Ag, Au and bimetallic nanoparticles using *Piper pedicellatum* C.DC: green chemistry approach. *Colloids and surfaces. B, Biointerfaces.* 102, 627–634. <https://doi.org/10.1016/j.colsurfb.2012.09.007>.
- Umbreit, W. W. and J. Stauffer, 1957. Manometric techniques, a manual describing methods applicable to the study of tissues metabolism.
- Wang, Q., Chen, F., Guo, L., et al., 2019. Nanoalloying effects on the catalytic activity of the formate oxidation reaction over AgPd and AgCuPd aerogels. *J. Mater. Chem. A* 7 (27), 16122–16135. <https://doi.org/10.1039/C9TA00664H>.
- Yadi, M., Azizi, M., Dianat-Moghadam, H., et al., 2022. Antibacterial activity of green gold and silver nanoparticles using ginger root extract. *Bioprocess Biosyst. Eng.* 45 (12), 1905–1917.